Journal of Structural Geology 35 (2012) 40–50

Contents lists available at SciVerse ScienceDirect

Journal of Structural Geology

journal homepage: www.elsevier.com/locate/jsg

Geometric consequences of ductile fabric development from brittle shear faults in mafic melt sheets: Evidence from the Sudbury Igneous Complex, Canada

Iris Lenauer, Ulrich Riller*

School of Geography and Earth Sciences, McMaster University, 1280 Main Street West, Hamilton, ON, Canada L8S 4K1

ARTICLE INFO

Article history:
Received 14 December 2010
Received in revised form
19 September 2011
Accepted 19 November 2011
Available online 29 November 2011

Keywords:
Mechanical weakening
Rotation
Brittle deformation
Ductile deformation
Fabric development
Sudbury Basin

ABSTRACT

Compared to felsic igneous rocks the genetic relationship between brittle and ductile fabric development and its influence on the geometry of deformed mafic melt sheets has received little attention in structural analyses. We explore these relationships using the Sudbury Igneous Complex (SIC) as an example. The SIC is the relic of a layered impact melt sheet that was transformed into a fold basin, the Sudbury Basin, during Paleoproterozoic deformation at the southern margin of the Archean Superior Province. We studied brittle and ductile strain fabrics on the outcrop and map scales in the southern Sudbury Basin, notably in the Norite and Quartz Gabbro layers of the SIC. Here, deformation is heterogeneous and occurred under variable rheological conditions, evident by the development of brittle shear fractures, brittle-ductile shear zones and pervasive ductile strain. The mineral fabrics formed under low- to middle greenschist-facies metamorphism, whereby brittle deformation caused hydrolytic weakening and ductile fabric development. Principal strain axes inferred from all structural elements are collinear and point to a single deformation regime that led to thinning of SIC layers during progressive deformation. Ductile fabric development profoundly influenced the orientation of SIC material planes, such as lithological contacts and magmatic mineral fabrics. More specifically, these planar structural elements are steep where the SIC underwent large magnitudes of thinning, i.e., in the south limb of the Sudbury Basin. Here, the actual tilt component of material planes is likely smaller than its maximum total rotation (60°) inferred from inclined igneous layering in the Norite. Our field-based study shows that ductile fabric development from brittle faults can have a profound influence on the rotational components of primary material planes in deformed igneous melt sheets.

1. Introduction

The formation of brittle shear faults in orogenic belts is usually considered to postdate ductile fabric development (e.g., Watts and Williams, 1979). As such, shear fractures are interpreted to record late stages of orogenic deformation. However, in initially isotropic rocks, notably granitoid bodies, brittle fractures have been documented to coalesce into zones of brittle-ductile or ductile deformation (Segall and Simpson, 1986; Bürgmann and Pollard, 1994; Tourigny and Tremblay, 1997; Pennacchioni, 2005). Thus, brittle faults may form during or even precede ductile deformation in granitoid rocks. As evidence for the existence of precursor brittle fractures is likely erased by subsequent pervasive crystal plastic deformation in orogenic belts (Means, 1989), the significance of small-scale shear fractures for accomplishing regional deformation of igneous rock bodies may have been largely underestimated. Despite the evidence for the development of isolated ductile shear zones from brittle precursor faults in granitoid rocks, it remains to be elucidated to what extent this process operates in mafic igneous rocks. Moreover, the kinematic effects of such fabric development on the geometry of deformed (mafic) igneous sheets have received little attention by structural analysts. Here we report on the genetic relationship between brittle and ductile fabric development and its influence on the melt sheet geometry using the Sudbury Igneous Complex, Canada, as an example. Because the Complex is layered, well-exposed and heterogeneously deformed, it lends itself excellently for this study.

The Sudbury Basin (Brocoum and Dalziel, 1974; Pye et al., 1984) is considered as the central portion of the Sudbury Impact Structure (Butler, 1994; Riller, 2005; Grieve et al., 2008). The Basin is made up of the Main Mass of the Sudbury Igneous Complex (SIC), the relic of an impact melt sheet (Grieve et al., 1991; Deutsch et al., 1995) dated at 1.85 Ga (Krogh et al., 1984), clast-melt breccias of the overlying Onaping Formation (Peredery and Morrison, 1984; Grieve et al., 2010), and post-impact sedimentary rocks (Fig. 1). Cu–Ni sulphide deposits are concentrated chiefly at the base of the SIC in the so-called Sublayer and adjacent rock (e.g., Keays and Lightfoot,

* Corresponding author. Tel.: +1 905 525 9140x26365; fax: +1 905 546 0463.
E-mail address: rilleru@mcmaster.ca (U. Riller).

0191-8141/$ – see front matter © 2011 Elsevier Ltd. All rights reserved.
doi:10.1016/j.jsg.2011.11.012

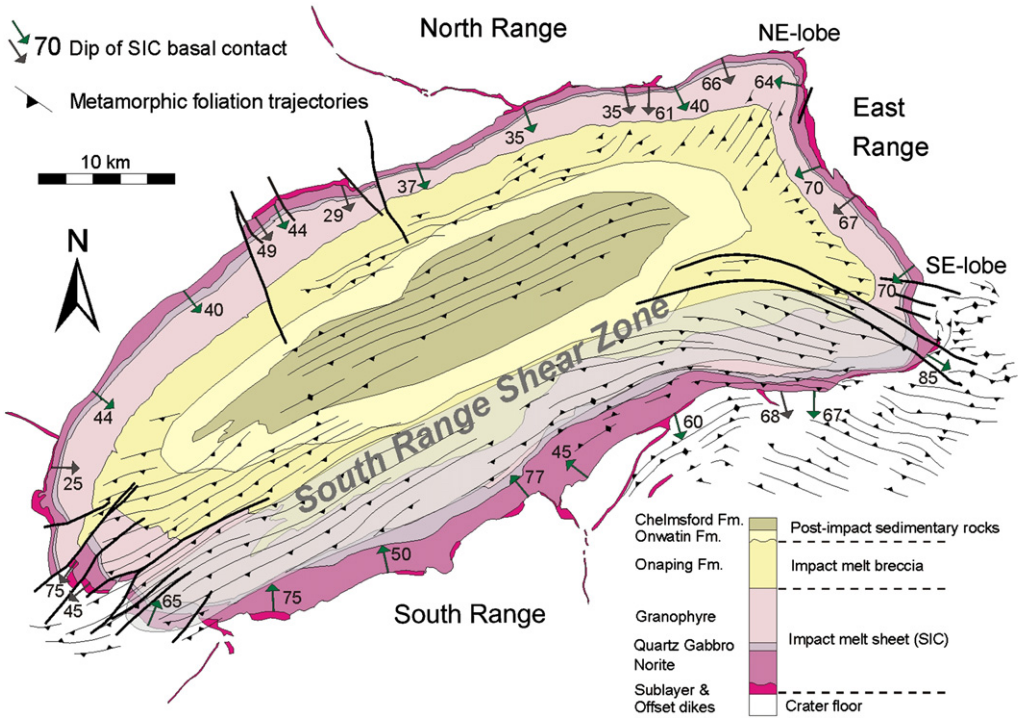

Fig. 1. Simplified geological map of the Sudbury Basin showing first-order structural characteristics (modified from Cowan et al., 1999). Dip magnitudes (numbers) of basal SIC contact segments are from Ames et al. (2005) and Dreuse et al. (2010) (green and black arrows, respectively). (For interpretation of the references to colour in this figure legend, the reader is referred to the web version of this article.)

2004; Ames and Farrow, 2007) and made the Sudbury Basin a world-class mining camp.

The synformal geometry of the SIC has been attributed to sagging of the melt sheet upon cooling (Peredery and Morrison, 1984) or is considered as primary (Cowan et al., 1999). More recent structural studies suggest, however, that this geometry is due to post-impact, non-cylindrical folding (Cowan and Schwerdtner, 1994; Riller et al., 1998; Riller, 2005; Klimczak et al., 2007; Halls, 2009; Dreuse et al., 2010). Due to the highly variable crater floor topography (Dreuse et al., 2010), the orientation of the lower SIC contact, notably of the southern Sudbury Basin, cannot be used to constrain rotation magnitudes of the SIC. Furthermore, internal contacts of the SIC are non-parallel at surface (Fig. 1). In particular, it is unclear whether this configuration constitutes the original orientation of the lithological contacts, or whether deformation modified the contact geometry.

To better understand the mechanisms of fabric development, including rotational components of deformation, in the southern SIC, we analyzed the orientation and spatial distribution of igneous and metamorphic mineral fabrics as well as outcrop-scale fold structures in the field. These analyses are complemented by inversion of small-scale, brittle-ductile shear faults from which we infer shortening directions during deformation of the SIC and its host rocks. Collectively, these data allow us to characterize the deformation mechanisms by which the SIC changed shape and its mechanical behavior during deformation. Our study pertains directly to understanding the deformation of, and strain localization in, mafic melt sheets at upper crustal levels.

2. Tectonic setting of the Sudbury Basin

At surface, the SIC forms morphological ranges, i.e., the North Range, the South Range and the East Range (Fig. 1). The North Range and the East Range are underlain by high-grade metamorphic and granitoid rocks of the Archean Superior Province (Card et al., 1972). These rocks formed at approximately 2.71 Ga and were affected by upper amphibolite- to granulite-facies metamorphism at around 2.65 Ga (Krogh et al., 1984). The South Range of the SIC overlies metavolcanic and metasedimentary rocks of the Huronian Supergroup which were deposited onto Archean rocks between 2.45 Ga (age of the Copper Cliff Formation: Krogh et al., 1984) and 2.21 Ga (Nipissing diabase intrusion: Corfu and Andrews, 1986). During this time interval Huronian metasedimentary rocks were deposited, deformed and metamorphosed to amphibolite-facies and intruded by the Creighton and Murray Plutons, which border the southern flank of the Sudbury Basin (Card et al., 1972; Card, 1978; Riller and Schwerdtner, 1997; Riller et al., 1999).

The SIC and Huronian rocks were affected by various Proterozoic pulses of deformation. Deformation of the SIC commenced likely during its cooling (Klimczak et al., 2007) but peak metamorphism and deformation of the SIC is thought to have occurred under prograde conditions (Fleet et al., 1987). New geochronologic and thermochronologic evidence suggests that significant post-impact deformation and metamorphism of Huronian rocks occurred at about 1.76 to 1.74 Ga (Piercey et al., 2007) and was likely associated with the emplacement of 1.74 Ga granitoid plutons (Easton, 2000). Deformation zones at the base of the South Range Norite were dated at ca. 1.65 Ga (Bailey et al., 2004). Proximity and orientation of the long axis of the Sudbury Basin to the NE-striking Grenville Front led some workers to invoke that the Basin was shaped by late Proterozoic Grenvillian tectonism (Dietz, 1964; Card et al., 1984; Fueten and Redmond, 1997; Spray et al., 2004). This is, however, at variance with the presence of unstrained diabase dikes of the 1.23 Ga Sudbury swarm (Gates and Hurley, 1973) in the Sudbury area (Brocoum and Dalziel, 1974). Thus, the age of Basin formation is still uncertain.

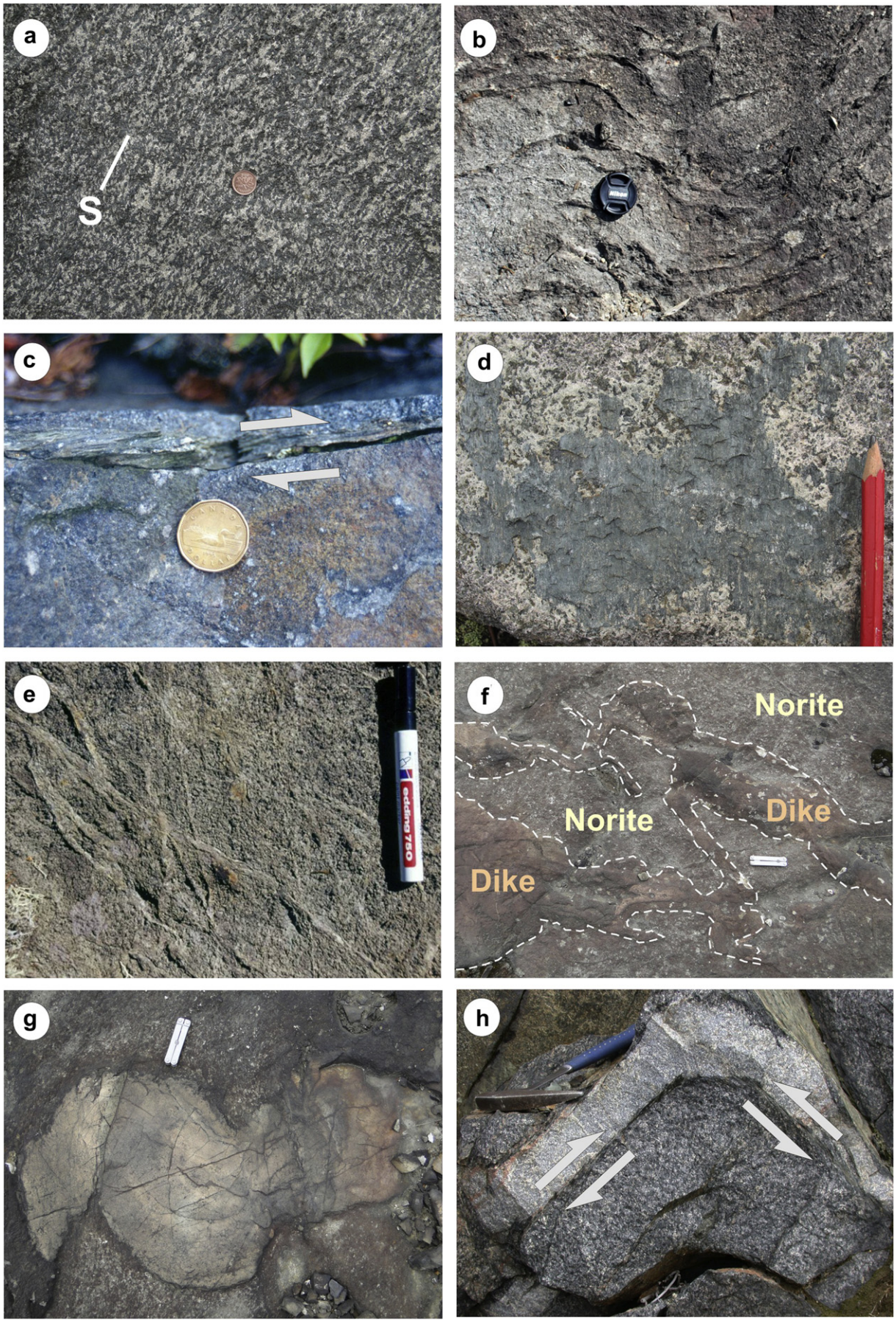
a
S
b
c
d
e
f
Norite
Norite
Dike
Dike
g
h

3. Structural characteristics of the Sudbury Basin

The Main Mass of the SIC is made up of petrographically distinct layers that are traditionally known as Norite, Quartz Gabbro and Granophyre (Fig. 1). Collectively, these layers are characterized by igneous and metamorphic mineral shape fabrics, the intensity and orientation of which vary with location. Much of the Sudbury Basin and adjacent Huronian host rocks were affected by deformation, the metamorphic grade of which varies from greenschist-facies in the North Range to lower amphibolite-facies in the South Range (Card, 1978; Thomson et al., 1985; Fleet et al., 1987). This led to the development of mesoscopic planar (S) and linear (L) mineral shape fabrics, the intensity of which decrease generally toward the north in the Sudbury area.

Except at the NE-lobe and SE-lobe of the Sudbury Basin (Fig. 1), planar metamorphic mineral shape fabrics strike parallel to the long axis of the Basin and are either subvertical or dip southward (Cowan, 1996). In the lobes, the shape fabrics are axial-planar to the plan view curvature of the SIC (Cowan, 1999) pointing to a fold origin of the two lobes (Cowan and Schwerdtner, 1994; Riller, 2005; Klimczak et al., 2007). In post-impact sedimentary rocks, planar fabrics developed as a slaty cleavage that is axial planar to doubly plunging, open similar and concentric folds of bedding planes (Rousell, 1984).

The South Range Shear Zone (SRSZ), a SE-dipping ductile deformation zone, is the most prominent structural element of the Sudbury Basin (Rousell, 1975; Shanks and Schwerdtner, 1991). Mineral fabrics of the shear zone display L-S geometry and formed mostly at, or near, the contact of the Granophyre and Onaping Formation (Fig. 1). Reverse sense-of-shear on the SRSZ translated the South Range approximately 8–13 km toward the NW (Shanks and Schwerdtner, 1991). The SRSZ formed apparently under lower amphibolite-facies metamorphic conditions and was overprinted by small-scale, brittle-ductile shear faults, which formed at mid greenschist-facies metamorphic conditions (Fleet et al., 1987).

The extent to which the South Range Norite was affected by deformation has not been studied in detail. Large portions of the South Range Norite are reported to be unstrained (Riller, 2005) and display igneous mineral fabrics characterized by a granular texture and hypidiomorphic plagioclase and hypersthene (Naldrett and Hewins, 1984; Thomson et al., 1985). The intercumulus mineral phases consist of augite, hornblende, quartz, titanomagnetite and biotite (Thomson et al., 1985). Naldrett et al. (1970) document metamorphic alteration of the Norite from the East Range and the South Range. In these areas Thomson et al. (1985) distinguish between the Black Norite, in which hypersthene and augite are preserved, and the Green Norite, which shows a metamorphic mineral assemblage of amphibole, epidote, biotite, albite and quartz. This mineral assemblage is consistent with prograde metamorphism to amphibolite-facies, known from Huronian host rock of the South Range (Fleet et al., 1987).

4. Results

4.1. Igneous fabrics

Igneous mineral fabrics of the South Range Norite are planar and consist of subhedral plagioclase, orthopyroxene and to some extent amphibole. Collectively, the fabric defined by these mineral phases is reminiscent of a cumulus texture (Fig. 2a). Plagioclase has andesine composition, shows twin lamellae, and is zoned, evident by the increase in sodium content towards crystal margins (Fleet and Barnett, 1978). Similarly, amphibole is zoned, apparent by cores of green hornblende rimmed by blue-green hornblende (Fleet and Barnett, 1978). It is noteworthy that none of these mineral phases form a mineral lineation.

Minerals indicative of metamorphism and hydrothermal alteration are known to have affected much of the South Range Norite. For example, epidote and scapolite occupy grain boundaries, notably between plagioclase and amphibole, replace plagioclase cores and coat fractures (Thomson et al., 1985). Similarly, talc replaces hypersthene cores and is found in fractures cutting bronzite. Hypersthene is rimmed by actinolitic hornblende and brown edenite is selectively replaced by blue-green actinolitic hornblende (Fleet et al., 1987). Chlorite, epidote and quartz decorate brittle fractures (see section 4.4). Despite metamorphic transformation of the Norite at the grain scale, primary igneous fabrics are generally preserved well enough to be visible in outcrop (Fleet et al., 1987).

Although often faint in outcrop, igneous layering can be observed throughout the South Range Norite. The orientation of planar igneous fabrics was mapped in the South Range Norite at 276 stations (Figs. 3a and 4a, b). For a better appraisal of along-strike fabric variation, the orientation of planar igneous fabrics was grouped into two zones, the Western Zone and the Eastern Zone, defined by NE-SW strike and E-W strike of SIC contacts, respectively (Fig. 3a). Assuming that layering in the SIC formed by gravitational settling (Naldrett et al., 1970) and was sub-horizontal prior to deformation, inclined planar igneous fabrics can be used to infer total rotation magnitudes of the South Range SIC. Planar igneous fabrics dip moderately toward the NW in the Western Zone (Fig. 4a) and toward the N in the Eastern Zone (Fig. 4b) and strike parallel to SIC contacts (Fig. 3a). The dip of planar igneous fabrics suggests that the South Range SIC was tilted by approximately 40°–60° toward the NW in the Western Zone and about the same magnitude toward the N in the Eastern Zone (Fig. 4a, b).

4.2. Metamorphic fabrics

The South Range SIC and adjacent Onaping Formation display metamorphic mineral fabrics, the orientations of which were recorded at a total of 349 stations (Figs. 3b and 4d, e, f). Except for in the South Range Shear Zone (Shanks and Schwerdtner, 1991), the mineral fabrics in the SIC have planar geometry and are either defined by the shape-preferred orientation of amphibole and potassium feldspar or by biotite and chlorite (Fig. 2c, d). In outcrops, in which both metamorphic mineral assemblages are present, fabrics defined by chlorite and biotite display the same orientation as fabrics made up mostly of amphibole. This allowed us to reliably distinguish between metamorphic mineral fabrics and igneous layering, as the latter is defined by subhedral plagioclase and orthopyroxene in the South Range Norite. Moreover, distinction between the two fabric types is corroborated by the fact that the Onaping Formation is devoid of planar igneous fabrics and that the

Fig. 2. Structural field characteristics of the South Range SIC. (a) Trace of planar igneous mineral fabrics (S) in Quartz Gabbro defined by subhedral plagioclase (white) and pyroxene transformed to actinolite (dark green). (b) Folded brittle shear faults in Norite. (c) Small-scale, brittle-ductile shear zone in Norite in profile plane. Note obliquity between metamorphic foliation defined by chlorite flakes and the zone margins. Half-arrows indicate sense-of-slip. (d) Brittle shear fault surface decorated by chlorite fibres. (e) Anastomosing pattern of small-scale chloritic shear zones in Norite. (f) Irregular shaped granitoid dike in Norite. Stippled lines delineate dike margins. (g) Buckled granitoid dike in Norite. Pocket knife is parallel to the trace of the shape-preferred orientation of metamorphic minerals in the Norite. (h) Folded granitoid dike in Quartz Gabbro. The dike margins of the fold limbs are reused as brittle-ductile slip surfaces. Half arrows indicate sense-of-slip. Note cuspate-lobate contact geometry in (g) and (h). (For interpretation of the references to colour in this figure legend, the reader is referred to the web version of this article.)

orientation of metamorphic mineral fabrics in the Onaping is akin to that mapped in the South Range SIC (Fig. 4d, e, f). Metamorphic and igneous mineral fabrics may be present in the same outcrops but generally display different orientations.

The orientation of planar metamorphic fabrics varies with position in the South Range SIC, notably in the Norite (Fig. 3b). Near the contact of the Onaping Formation with the Granophyre, which lies within the SRSZ (Fig. 1), and at the upper and lower contacts of the Quartz Gabbro, fabrics dip moderately to steeply southward and strike parallel to these contacts (Fig. 4d–f). By contrast, the strike of planar mineral fabrics in the Norite, in particular close to its basal contact, is highly variable and often at high angles to the SIC-footwall contacts (Fig. 3b). The variation in planar fabric orientation can be explained by the map-scale strain gradient associated with the SRSZ. Specifically, away from the SRSZ, i.e., in the basal Norite, highly variable fabric orientations point to low levels of map-scale strain as opposed to high strain levels indicated by the more uniform orientation of planar fabrics in the SRSZ.

In the Western Zone, foliation planes in the Onaping Formation dip at moderate angles uniformly to the S (Fig. 4d). In the adjacent Granophyre two clusters of foliation orientations are apparent (Fig. 4e). Here, a well-defined cluster indicates steeply south-dipping foliation planes, whereas a less pronounced one represents steeply north-dipping planes. A bimodal orientation of foliation planes, i.e., steeply north- and steeply southward dipping planes, is well apparent in the Norite and Quartz Gabbro (Fig. 4f). Thus, metamorphic foliation seems to change systematically from a conjugate pattern in the Norite and Quartz Gabbro to uniformly south-dipping planes in the Onaping Formation. This points to a progressive change from co-axial to non-co-axial deformation toward the SRSZ.

Metamorphic fabric development varies with location in the South Range. Fabric development can be assessed by the number of shear planes per area in a given outcrop (Fig. 5) and ranges from isolated, few millimeter-wide deformation zones (Fig. 2c, d, 5a) to pervasively foliated rock (Fig. 2g). At low spatial density, shear fractures are spaced decimeters to meters apart and are observed to be planar (Fig. 5a). In these locations, intersections between fractures are at high angles to each other and show little offset (Fig. 5a). At higher spatial densities, shear fractures are conjugate to each other and connect to millimeter- to centimeter-wide ductile shear zones (Fig. 5b, c). The foliation in these zones is mostly defined by the shape-preferred orientation of chlorite and biotite, and is oblique to shear zone margins (Fig. 2c).

The variation in metamorphic fabric development can be used to crudely map deformation intensity in the South Range SIC (Fig. 3c). Outcrops characterized by the sporadic presence of thin seams of metamorphic minerals, notably chlorite fibers, which nucleate in and decorate brittle shear fractures (Fig. 2d), form zones of low deformation intensity. Outcrops replete with centimeter-wide shear zones form zones of moderate deformation intensity. The shear zones often have anastomosing geometry (Fig. 2e) and coalesce to form meter-wide foliated zones in areas of high deformation intensity. Outcrops characterized by pervasive metamorphic foliation form zones of very high deformation intensity.

Heterogeneity in metamorphic fabric development as seen on the outcrop scale is also evident on the map scale. Here, deformation intensity varies on the hundred-meter to kilometer scale (Fig. 3c). In places, outcrops characterized by high deformation intensity connect to kilometer-scale zones of continuous deformation. In particular, there is a laterally coherent NNE-striking zone of enhanced deformation north of the eastern Creighton Pluton (Fig. 3a, c), henceforth referred to as the Whitewater Lake Fault Zone (WFZ). On outcrop scale the WFZ is characterized by pervasive, subvertical and symmetric anastomosing planar metamorphic mineral fabrics, which are devoid of mineral lineations. The zone transects the Quartz Gabbro where its upper and lower contacts deviate from their overall ENE strike toward the NE (Fig. 3a). The strike separation displayed by these contacts agrees with the sigmoidal curvature of metamorphic foliation trajectories associated with the WFZ (Fig. 3b) and may indicate a sinistral shear component resolved on the WFZ. Thus, the WFZ forms a broad zone of continuous deformation that displaces the South Range SIC.

4.3. Folded granitoid dikes

The South Range Norite contains dike- and pod-like bodies of granitoid composition that range in thickness from a few millimeters to decimeters and can be traced up to tens of meters. The bodies are likely derived from the nearby ca. 2.3 Ga Creighton and Murray Plutons (Fig. 3a). The shapes of the granitoid bodies are highly irregular and have wispy apophyses (Fig. 2f), reminiscent of magma mingling. This suggests that the granitoid bodies intruded the Norite as back injections when the Norite was a melt.

The granitoid bodies are tightly to isoclinally folded. The folds are associated with an axial-planar fabric in the adjacent host rock (Fig. 2g) that is chiefly defined by the shape-preferred orientation of amphibole and biotite. The margins of folded dikes are lobate, whereas the host rock displays cusps (Fig. 2g, h). This indicates that the dikes were mechanically more competent than the host rock during folding. However, the dikes retained their structural coherence during this deformation, which indicates continuous deformation during shape change of the granitoid dikes.

Assuming that the folds of the granitoid dikes formed due to shortening orthogonal to their fold-axial planes, i.e., in the direction of the poles to these planes, local shortening directions for the South Range SIC were determined at 55 stations (Fig. 4g). Shortening directions in the Western Zone are mostly NW–SE and in agreement with left-lateral strike separation of SIC contacts on the WFZ, whereas shortening in the Eastern Zone is rather N–S (Fig. 3e). Thus, the shortening directions inferred from folded granitoid dikes are crudely orthogonal to the strike of the SIC contacts (Fig. 3e, f).

4.4. Brittle deformation

Small-scale brittle shear faults are pervasively developed in the South Range SIC and adjacent Huronian rocks. The fault planes are mostly decorated by chlorite fibers (Fig. 2d) and sporadically by fibrous quartz, calcite and biotite. In places, faults are associated with fault gouge or cohesive cataclasite. The sense-of-slip on the faults was determined by the polarity of stair-stepping geometry displayed by the mineral fibers, secondary Riedel fractures and displaced passive markers, such as granitoid dikes.

The orientation of 372 brittle fault surfaces and their respective striations were measured at 29 stations (Fig. 6, Table 1). The sense-of-slip was reliably determined for 200 fault surfaces. The fault populations consist chiefly of moderately SE- and NW-dipping conjugate reverse faults and N–S striking strike-slip faults (Fig. 6). Based on the orientation of fault surfaces, the orientation of mineral fibers and the sense-of-slip, principal axes of paleostress or infinitesimal strain can be calculated for a given fault population (Angelier, 1979). As displacement on the brittle fault surfaces is minimal, we interpret principal paleostress axes in terms of paleostrain axes.

The presence of conjugate fault sets calls for an analytical method that considers each fault plane individually. As some stations displayed a low number of fault planes with a reliable

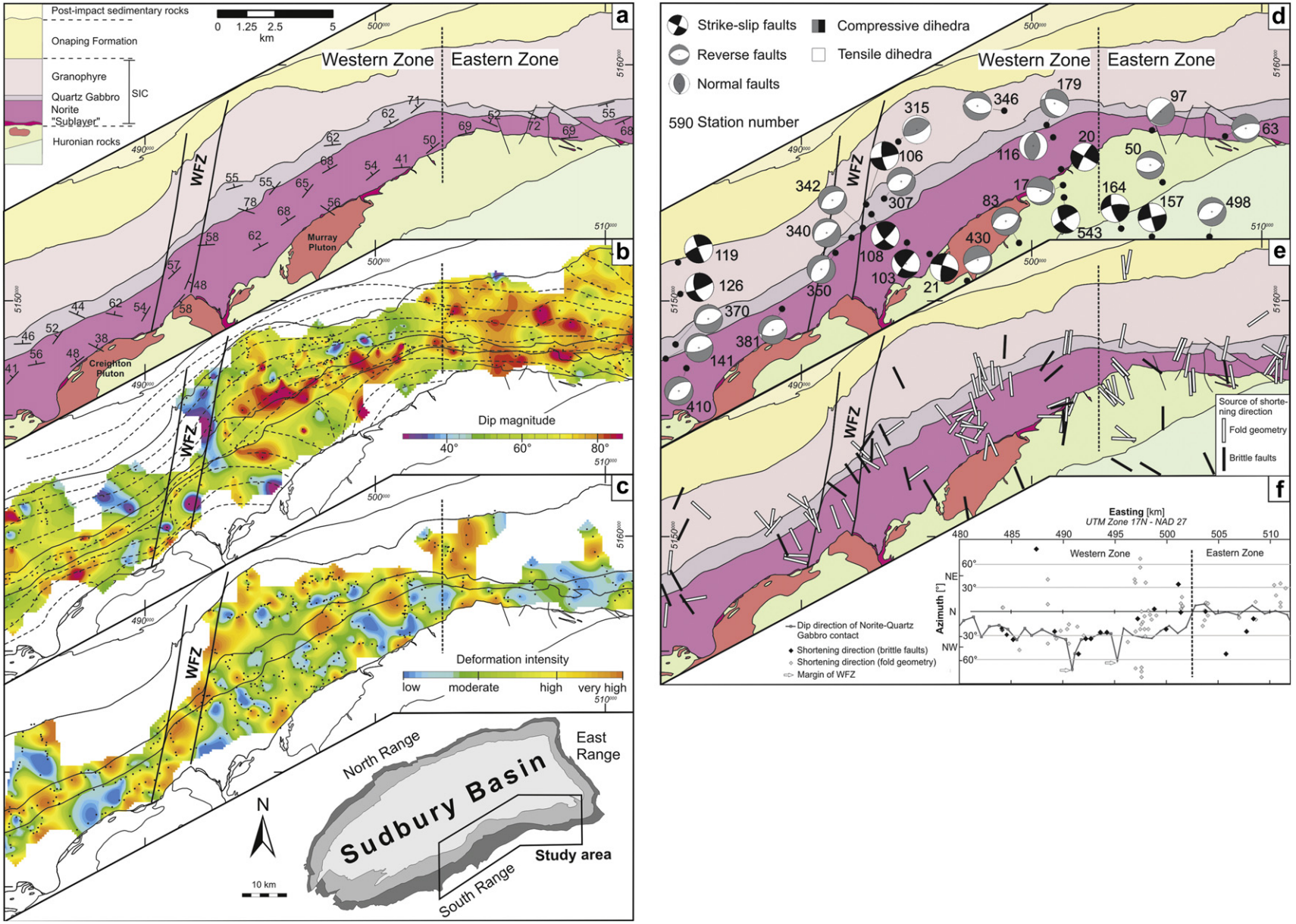

Fig. 3. Structure of the study area in the South Range SIC. WFZ: Whitewater Lake Fault Zone. (a) Simplified geological map showing averages of dip directions (symbols) and dip magnitudes (numbers) of igneous layering. (b) Strike trajectories of inclined planar metamorphic shape fabrics (including data by Ames et al., 2005) overlain on contoured dip magnitudes of fabrics. Note the large variation in fabric strike in the basal Norite as opposed to that at the contact of the Granophyre with the Onaping Formation. (c) Variation in intensity of metamorphic mineral fabrics. For definition and explanation of fabrics see text. Contours in (b) and (c) were created with a minimum curvature algorithm using a cell size of 100 m. Dots in (b) and (c) show location of stations the contouring is based on. (d) Map showing dihedra of shortening and extension inferred from the inversion of brittle shear faults using the Numerical Dynamic Analysis. Station numbers correspond to numbering of diagrams and principal strain axes shown in Fig. 5 and Table 1, respectively. (e) Directions of shortening inferred from brittle-fault analysis and fold geometry of granitoid dikes, projected onto the map plane. (f) Graph showing the along-strike variation in dip direction (azimuth) of the contact between Norite and Quartz Gabbro and shortening directions. The x-axis marks Easting coordinates. Note parallelism of shortening directions with dip direction of contact.

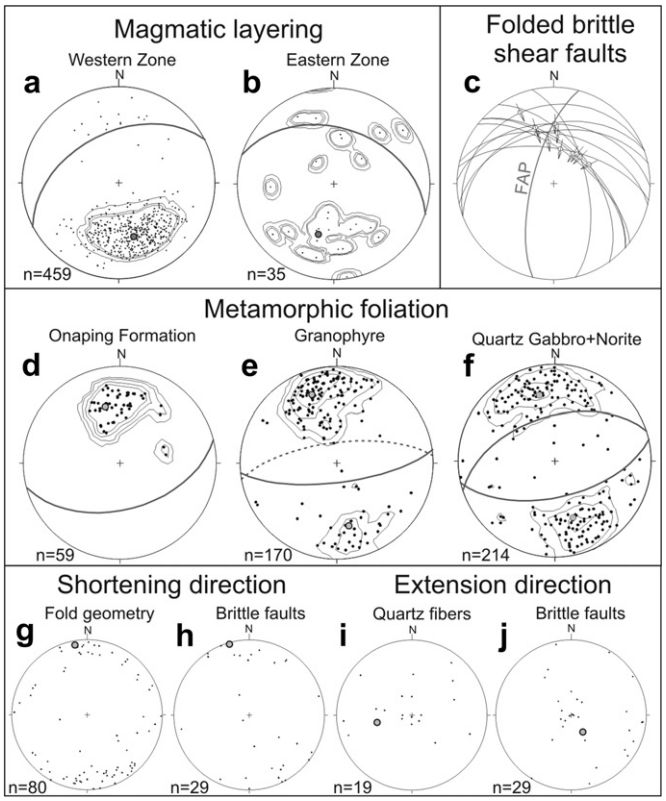

Fig. 4. Lower-hemisphere, equal-area projections of magmatic and metamorphic fabric elements of the South Range SIC. Large grey circles indicate means and *n* the respective number of measurements. (a) Poles to magmatic layering in the Western Zone. (b) Poles to magmatic layering in the Eastern Zone. (c) Orientation of folded brittle fault plane segments (great circles), respective sense-of-slip of hanging walls (arrows) and fold-axial plane (FAP). (d) Poles to metamorphic foliation in the Onaping Formation. (e) Poles to metamorphic foliation in the Granophyre. (f) Poles to metamorphic foliation in the Quartz Gabbro and Norite. Foliation planes in (d) to (f) are from the Western Zone. (g) Poles to fold-axial planes of granitoid dikes. (h) Shortening directions inferred from brittle shear faults. (i) Orientation of quartz fibers. (j) Extension directions inferred from brittle shear faults. Note co-linearity of mean directions in (g) and (h), and (i) and (j), respectively.

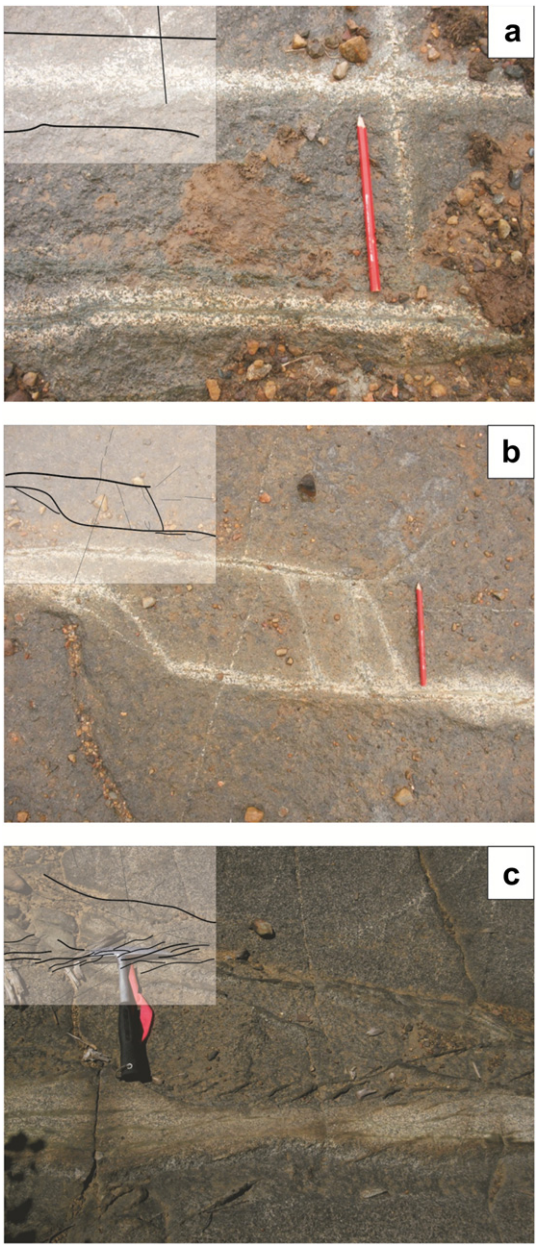

Fig. 5. Outcrop photos showing variable fracture densities and the coalescence of shear fractures into shear zones with increasing deformation intensity. Shear fractures are well evident by alteration halos. (a) Widely spaced fractures oriented at high angles to each other. (b) Isolated fractures coalescing to thin shear zone. (c) Shear zone characterized by sigmoidal brittle-ductile shear fractures in an outcrop containing a high fracture density.

sense-of-slip, the application of analytical methods searching for the best-fit reduced stress tensor is limited. For each fault population per station, the infinitesimal shortening and extension directions (Table 1) were calculated using the Numerical Dynamic Analysis (NDA: Spang, 1972). This method assigns to each fault plane a shear strain magnitude of 1. Furthermore, the angle between the maximum principal strain axes and the fault plane is identical for each fault population. For our analysis, we chose an angle of 30° between the maximal principal strain direction and the maximum resolved shear strain, which is within the limits of experimentally obtained values for this angle (Byerlee, 1968).

For each fault plane a set of shortening and extension directions is calculated in tensor form. The sum of all tensors divided by the number of fault planes results in the deviatoric strain tensor. The eigenvector and the eigenvalue of this tensor define the orientation of the principal strain directions ($\varepsilon_1 > \varepsilon_2 > \varepsilon_3$) and the strain ratio ($R_{strain}$). In addition, NDA gives the number of fault planes whose measured slip senses are opposite to the ones predicted by a particular solution ("nev" in Table 1).

Shortening axes plunge shallowly north- or southward at almost all stations (Figs. 4h and 6). The direction of extension is vertical in 16 stations, sub-horizontal at 10 stations and hybrid at 3 (Figs. 3d, 4j, 6). Subvertical extension during brittle deformation is also indicated by the orientation of fibrous quartz in extension veins (Fig. 4i). Analogous to the shortening directions inferred from granitoid dikes, shortening directions based on inversion of brittle shear faults are crudely orthogonal to the strike of SIC contacts and compatible with left-lateral displacement on the WFZ (Fig. 3d, e).

Finally, it should be noted that brittle fault surfaces in the Norite of the Eastern Zone are sporadically folded (Fig. 2b). Fault planes decorated with quartz and chlorite are spaced several centimeters apart and display open folds. As a consequence of folding, mineral fibers on individual folded fault planes are fanning around the respective fold hinge zone (Fig. 4c). This suggests that brittle faulting preceded in places continuous deformation accomplished by folding and foliation development.

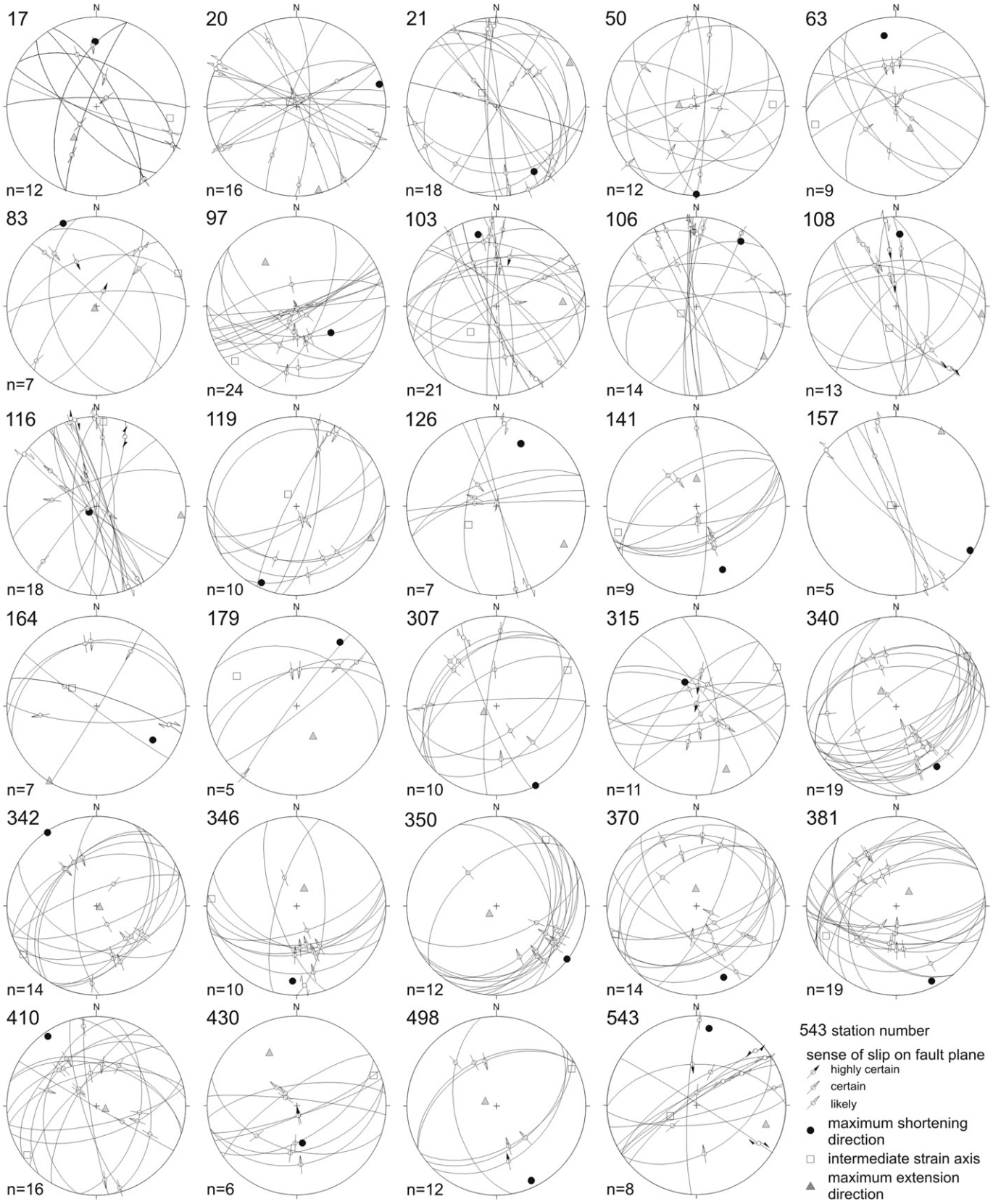

Fig. 6. Lower-hemisphere equal-area projections showing the orientation of brittle faults (great circles) and respective sense-of-slip of hanging walls (arrows) as well as principal strain axes inferred from Numerical Dynamic Analysis (Table 1).

Table 1
Quantities of brittle deformation inferred from Numerical Dynamic Analysis. Orientation of shortening (ε_3) and extension (ε_1) axes is given as dip direction/dip. R_{Strain} is the strain ratio, # denotes the number of fault planes per station and *nev* is the number of fault planes whose measured slip senses are opposite to the ones predicted by a particular solution.

Station	Easting	Northing	ε_3	ε_2	ε_1	R_{Strain}	#hf	*nev*
17	501398	5154995	359/28	099/18	217/56	0.35	24	0
20	501438	5154449	075/05	305/83	165/06	0.72	16	1
21	495904	5151735	150/17	314/72	058/04	0.29	18	3
50	503787	5157118	180/02	089/15	216/75	0.83	12	0
63	508415	5157102	351/21	257/09	146/67	0.57	9	0
83	499974	5152541	338/01	068/02	230/88	0.62	7	1
97	505765	5157393	127/49	228/09	325/39	0.60	24	4
103	494624	5152482	346/19	225/56	086/27	0.41	21	0
106	492853	5154140	034/13	246/75	126/08	0.53	14	1
108	493081	5153715	002/21	197/69	095/05	0.10	13	0
116	501305	5155672	229/81	005/06	096/06	0.87	18	3
119	484749	5151557	204/07	325/77	113/11	0.48	10	0
126	484446	5149476	026/24	244/61	123/16	0.62	8	1
141	484147	5147448	157/24	251/09	000/64	0.53	9	0
157	504039	5153825	121/04	280/86	031/02	0.50	5	0
164	502588	5154106	121/27	306/63	212/02	0.66	7	0
179	501165	5157901	034/15	297/26	151/59	0.72	5	0
307	493626	5154397	154/01	063/12	248/78	0.33	10	1
315	494258	5156862	334/66	064/00	154/24	0.18	11	0
340	492216	5152694	146/20	055/03	317/70	0.52	19	0
342	492714	5153124	326/02	236/02	098/87	0.48	14	0
346	498842	5158206	183/17	275/06	022/72	0.42	10	0
350	491513	5152040	127/01	037/09	225/81	0.50	12	0
370	484583	5148069	151/00	241/02	056/88	0.83	14	0
381	489212	5149620	155/08	247/16	040/72	0.68	19	0
410	485203	5147183	325/06	235/06	102/82	0.79	16	1
430	497233	5150617	171/55	069/09	333/33	0.51	9	1
498	507750	5152161	155/09	064/07	295/79	0.50	6	0
543	501416	5154448	009/14	248/64	105/21	0.25	12	0

5. Interpretation and significance of structural data

Our structural analysis indicates that the South Range SIC, particularly the Norite, underwent heterogeneous deformation, evident by the development and spatial distribution of centimeter- to the kilometer-scale structures. Specifically, we examined the orientation of (1) planar metamorphic mineral fabrics, (2) quartz fibres in extension veins, (3) folds in granitoid dikes, (4) small-scale brittle shear faults and (5) kilometer-scale deformation zones. The orientation and kinematics of these structures indicate that the South Range SIC underwent substantial layer-parallel stretching and layer-normal shortening, i.e., thinning.

There is a marked variation in shortening directions evident from fault-slip analysis, fold geometry of granitoid dikes and orientation of planar metamorphic shape fabrics that correlates with the strike of the SIC contacts (Fig. 3b, e, f). Specifically, shortening directions are oriented N–S in the E–W trending Eastern Zone, whereas the NE-SW trending Western Zone is dominated by NW-SE trending shortening directions. Thus, shortening directions are approximately perpendicular to the SIC contacts, whereas extension directions are mostly vertical (Fig. 3d). This geometry of local shortening and extension axes corroborates thinning of the South Range SIC.

The shortening and extension axes inferred from the orientation of metamorphic foliation surfaces, geometry of granitoid dikes, kinematics of brittle-ductile shear faults and orientation of quartz fibers in extension fractures are largely collinear (Fig. 4). Thus, the strain fabrics formed under variable rheological conditions (see below), but under a single deformation regime during progressive shortening. However, it remains to be ascertained whether deformation of the South Range SIC under these conditions occurred during cooling (Riller, 2005; Klimczak et al., 2007) or during prograde regional metamorphism (Thomson et al., 1985) of the SIC.

The presence of folded brittle-ductile fault planes in the Norite suggests that discontinuous deformation of the SIC preceded continuous deformation in many places. This is also evident by anastomosing, chlorite- and biotite-coated shear fractures coalescing to form ductile shear zones in the Norite and Quartz Gabbro (Fig. 2e). Collectively, this indicates that zones of pervasive foliation development formed initially from localized brittle shear faults (e.g., Pennacchioni, 2005). Evidently, brittle faults in the Norite and Quartz Gabbro lead to localized hydration and transformation of mafic minerals to chlorite and biotite in fault rock. This indicates low- to middle greenschist-facies metamorphic conditions during deformation. Such low-temperature, hydrolytic weakening (Kronenberg et al., 1990) caused widening of brittle shear fractures to hydrated shear faults that ultimately coalesced into broad ductile deformation zones during progressive deformation (Figs. 5 and 7). This mechanism of metamorphic foliation development by coalescence of hydrated brittle-ductile shear bands has also been documented in initially isotropic granitoid rock (Choukroune and Gapais, 1983; Christiansen and Pollard, 1997).

Bulk NW-SE shortening in the South Range SIC is compatible with large-scale folding of the SIC and the kinematics of the SRSZ. The SRSZ may have formed independently of folding (Milkereit et al., 1992; Wu et al., 1994; Boerner et al., 2000) or as a consequence of folding-induced strain (Card and Jackson, 1995). The map-scale variation in orientation of metamorphic foliation (Fig. 3b) and the northward increase in non-coaxiality of deformation (Fig. 4d–f) suggest that deformation in the South Range SIC is kinematically related to the formation of the SRSZ. The fact that only a single deformation regime can be discerned from the strain fabrics may, therefore, indicate that large-scale folding of the SIC occurred contemporaneously with activity of the SRSZ (Fig. 7). This hypothesis agrees with the observed predominance of symmetric strain fabrics in the South Range SIC indicating flattening strains (Fig. 4e, f). Bulk thinning of the SIC as the main mechanism of

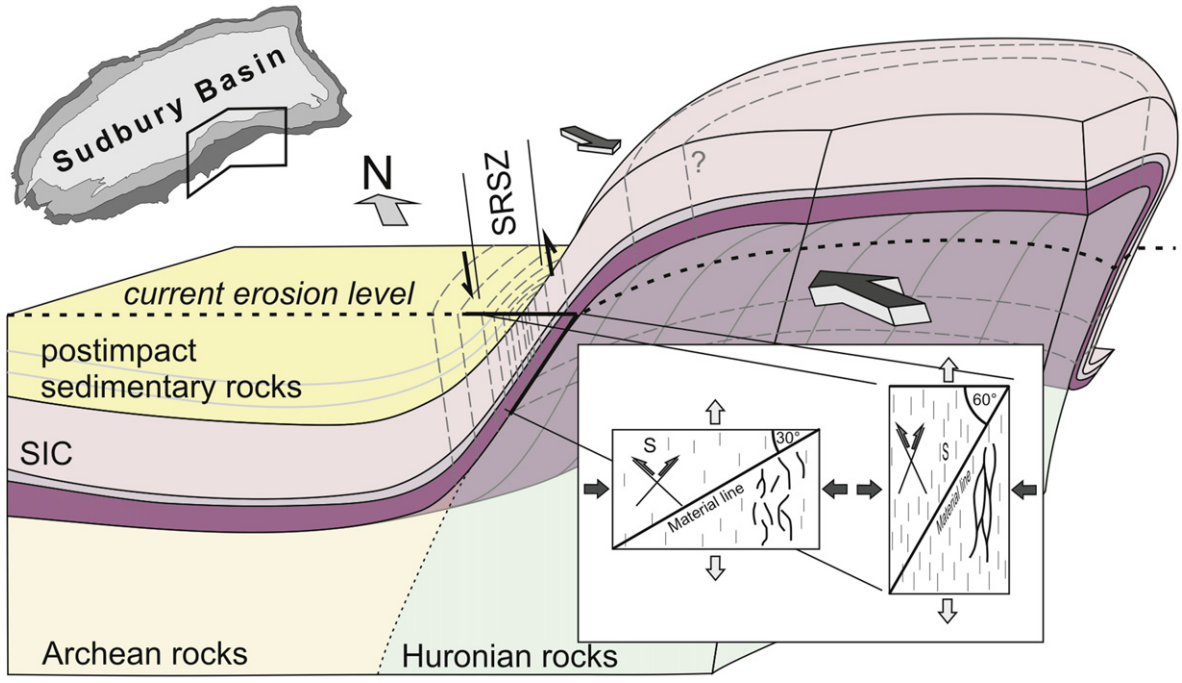

Fig. 7. Conceptual model showing structural characteristics of the deformed South Range SIC. The South Range Shear Zone (SRSZ) forms as a consequence of folding-induced strain that leads to thinning of the SIC in the steep short limb of an asymmetric anticline-syncline pair. Traces of foliation surfaces are shown as grey stippled lines. Inset shows the shear-induced rotation of material surfaces, such as conjugate shear faults, anastomosing brittle-ductile shear zones, foliation surfaces (S) and inclined contacts, after 40% of bulk coaxial shortening (dark arrows) and respective extension (light arrows). Note steepening of material line representing the basal SIC contact by about 30° as a consequence of overall thinning of the SIC and reduction in the angle between conjugate structures. The orientation of foliation surfaces does not change with respect to the principal axes of bulk strain.

deformation is compatible with geochemical profiles across the South Range SIC. These profiles are characterized by systematic variations in chemical trends showing no marked discontinuities (Lightfoot, 2009). Also, analog experiments by Riller et al. (2010) suggest that the formation of the SRSZ is a mechanical consequence of folding of the SIC (Card and Jackson, 1995).

The deformation fabrics recorded in the South Range Norite have important implications for understanding the magnitude and mechanism of rotation in the South Range. The total magnitude of rotation of the South Range SIC, as inferred from the orientation of igneous layering in the Norite, ranges from 40° to 60° (Fig. 4a). However, not all of this rotation magnitude may have been taken up by solid-body rotation, i.e., tilting of the South Range SIC. Layer-parallel thinning can enhance the dip of pre-existing inclined material surfaces, such as lithological contacts and primary layering, by shearing-induced rotation (inset in Fig. 7). This may well have enhanced the inclination of SIC contacts and igneous layering during N–S shortening in the South Range. Thus, the actual tilt component of the South Range at the current level of erosion is expected to be smaller than indicated by the inclination of igneous layering in the Norite (60°: Figs. 4a and 7). Accordingly, variable magnitudes of thinning can account for the observed difference in contact dips between the South Range and the North Range. In particular, dip magnitudes of SIC contacts are larger for the South Range than for the North Range (Fig. 1). Structural elements in the South Range SIC suggest that it constitutes the short, but highly strained, limb of an asymmetric, NW-verging km-scale anticline-syncline pair of the SIC (Fig. 7).

6. Conclusions

Deformation in the South Range SIC, notably the Norite and Quartz Gabbro, was accomplished by centimeter- to kilometer-scale structures, notably planar metamorphic mineral fabrics, tight to isoclinal folds in granitoid dikes, small-scale brittle shear faults and first-order ductile high-strain zones. Deformation was heterogeneous and occurred under variable rheological conditions but evidently under a single deformation regime. This suggests that shape change of the South Range SIC was achieved during folding of the SIC and concomitant reverse sense-of-shear on the SRSZ. Locally, brittle deformation preceded the development of pervasive planar metamorphic mineral fabrics and caused hydrolytic weakening of initially isotropic Norite and Quartz Gabbro. As a consequence, these units were thinned, which likely had a profound influence on the geometry and kinematics of deformation in the South Range SIC during overall NW–SE shortening. Most importantly, thinning of the South Range SIC enhanced the inclination of its contacts and igneous layering. This suggests that the actual tilt component of the South Range is smaller than the maximum rotation (60°) of the Norite as indicated by the dip of its igneous layering. Variable magnitudes of thinning of the SIC can account for differences in contact inclination of the North Range and the South Range. The structure of the latter is compatible with that of the short limb of a NW-verging, asymmetric fold.

Acknowledgments

This project was funded by Vale Inc., Copper Cliff, Ontario. Discussions with Lisa Gibson, Arnold Burton, Peter Lightfoot and Bill Morris improved the quality of this work significantly. A constructive review by Alain Vauchez is greatly appreciated.

References

Angelier, J., 1979. Determination of the mean principle directions of stresses for a given fault population. Tectonophysics, T17–T26.
Ames, D.E., Davidson, A., Buckle, J.L., Card, K.D., 2005. Geology, Sudbury Bedrock Compilation. Geological Survey of Canada, Ontario. Open File 4570, scale 1:50 000.

Ames, D.E., Farrow, C.E.G., 2007. Metallogeny of the Sudbury mining camp, Ontario. In: Goodfellow, W.D. (Ed.), Mineral Deposits of Canada- a Synthesis of Major Deposit Types, District Metallogeny, the Evolution of Geological Provinces and Exploration Methods. Geological Association of Canada Special Publication, vol. 5, pp. 329–350.

Bailey, J., Lafrance, B., McDonald, A., Fedorowich, J., Kamo, S., Archibald, D., 2004. Mazatzal-Labradorian-age (1.7–1.6 Ga) ductile deformation of the South Range Sudbury impact structure at the Thayer Lindsley mine, Ontario. Canadian Journal of Earth Sciences 41, 1491–1505.

Boerner, D.E., Milkereit, B., Wu, J., Salisbury, M., 2000. Seismic images and three-dimensional architecture of a Proterozoic shear zone in the Sudbury structure (Superior Province, Canada). Tectonics 19, 397–405.

Brocoum, S., Dalziel, I., 1974. Sudbury Basin, Southern Province, Grenville front, and Penokean orogeny. Geological Society of America Bulletin 85, 1571–1580.

Butler, H., 1994. Lineament analysis of the Sudbury multiring impact structure. Geological Society of America Special Paper 293, 319–329.

Bürgmann, R., Pollard, D.D., 1994. Strain accommodation about strike-slip-fault discontinuities in granitic rock under brittle-to-ductile conditions. Journal of Structural Geology 16, 1655–1674.

Byerlee, J.D., 1968. Brittle ductile transition in rock. Journal of Geophysical Research 73, 4741–4750.

Card, K.D., 1978. Geology of the Sudbury-Manitoulin area, District of Sudbury and Manitoulin. In: Ontario Geological Survey, Report, vol. 166, 238 p.

Card, K.D., Church, W.R., Franklin, J.M., Robertson, J.A., West, G.F., Young, G.M., 1972. The Southern Province. In: Price, R.A., Douglas, R.J.W. (Eds.), Variations in Tectonic Style in Canada. Geological Association of Canada Special Paper, vol. 8, pp. 335–380.

Card, K.D., Gupta, P.H., McGrath, P.H., Grant, F.S., 1984. Sudbury Structure: Its Regional Geological and Geophysical Setting. In: Pye, E.G., Naldrett, A.J., Giblin, P.E. (Eds.), The Geology and Ore Deposits of the Sudbury Structure. Special Publication 1, Ontario Geological Survey, Toronto, pp. 25–43.

Card, K.D., Jackson, S.L., 1995. Tectonics and Metallogeny of the Early Proterozoic Huronian Foldbelt and the Sudbury Structure of the Canadian Shield, Field Trip Guide Book. Geological Survey of Canada, Open File 3139, 55 p.

Choukroune, P., Gapais, D., 1983. Strain pattern in the Aar granite (Central Alps): orthogneiss developed by bulk inhomogeneous flattening. Journal of Structural Geology 5, 411–418.

Christiansen, P.P., Pollard, D.D., 1997. Nucleation, growth and structural development of mylonitic shear zones in granitic rock. Journal of Structural Geology 19, 1159–1172.

Corfu, F., Andrews, A.J., 1986. A U-Pb age for mineralized Nipissing diabase, Gowganda, Ontario. Canadian Journal of Earth Sciences 23, 107–109.

Cowan, E.J. 1996. Deformation of the eastern Sudbury basin. Ph.D. thesis, University of Toronto, 366 p.

Cowan, E.J., 1999. Magnetic fabric constraints on the initial geometry of the Sudbury Igneous Complex: a folded sheet or a basin-shaped igneous body? Tectonophysics 307, 135–162.

Cowan, E.J., Schwerdtner, W.M., 1994. Fold origin in the Sudbury basin. In: Lightfoot, P.C., Naldrett, A.J. (Eds.), Proceedings of the Sudbury - Noril'sk Symposium. Ontario Geological Survey, pp. 45–55. Special volume 5.

Cowan, E.J., Riller, U., Schwerdtner, W.M., 1999. Emplacement geometry of the Sudbury Igneous Complex: structural examination of a proposed impact melt-sheet. In: Dressler, B.O., Sharpton, V.L. (Eds.), Large Meteorite Impacts and Planetary Evolution II. GSA Special Paper 339. Geological Society of America, Boulder, pp. 399–418.

Deutsch, A., Grieve, R.A.F., Avermann, M., Bischoff, L., Brockmeyer, P., Buhl, D., Lakomy, R., Müller-Mohr, V., Ostermann, M., Stöffler, D., 1995. The Sudbury Structure (Ontario, Canada): a tectonically deformed multi-ring impact basin. Geologische Rundschau 84, 697–709.

Dietz, R., 1964. Sudbury structure as an astrobleme. Journal of Geology 72, 412–434.

Dreuse, R., Doman, D., Santimano, T., Riller, U., 2010. Crater-floor topography and impact melt sheet geometry of the Sudbury impact structure, Canada. Terra Nova 22, 463–469.

Easton, R.M., 2000. Metamorphism of the Canadian Shield, Ontario, Canada. II. Proterozoic metamorphic history. Canadian Mineralogist 38, 319–344.

Fleet, M.E., Barnett, R.L., 1978. Al^{iv}/Al^{vi} partitioning in calciferous amphiboles from the Frood mine, Sudbury, Ontario. Canadian Mineralogist 16, 527–532.

Fleet, M.E., Barnett, R.L., Morris, W.A., 1987. Prograde metamorphism of the Sudbury igneous complex. Canadian Mineralogist 25, 499–514.

Fueten, F., Redmond, D.J., 1997. Documentation of a 1450 Ma contractional orogeny preserved between the 1850 Ma Sudbury impact structure and the 1 Ga Grenville orogenic front, Ontario, Canada. Geological Society of America Bulletin 109, 268–279.

Gates, T.M., Hurley, P.M., 1973. Evaluation of Rb-Sr dating methods applied to the Matachewan, Abitibi, Mackenzie, and Sudbury dike swarms in Canada. Canadian Journal of Earth Sciences 10, 900–919.

Grieve, R., Stöffler, D., Deutsch, A., 1991. The Sudbury Structure - controversial or misunderstood. Journal of Geophysical Research 96, 22753–22764.

Grieve, R.A.F., Reimold, W.U., Morgan, J., Riller, U., Pilkington, M., 2008. Observations and interpretations at Vredefort, Sudbury and Chicxulub: towards an empirical model of terrestrial impact basin formation. Meteoritics and Planetary Science 43, 855–882.

Grieve, R.A.F., Ames, D.E., Morgan, J.V., Artemieva, N., 2010. The evolution of the Onaping formation at the Sudbury impact structure. Meteoritics and Planetary Science 45, 759–782.

Halls, H.C., 2009. A 100 km-long paleomagnetic traverse radial to the Sudbury Structure, Canada, and its bearing on Proterozoic deformation and metamorphism of the surrounding basement. Tectonophysics 474, 493–506.

Keays, R.R., Lightfoot, P.C., 2004. Formation of Ni-Cu-Platinum group element sulfide mineralization in the Sudbury impact melt sheet. Mineralogy and Petrology 82, 217–258.

Klimczak, C., Wittek, A., Doman, D., Riller, U., 2007. Fold origin of the NE-lobe of the Sudbury Basin, Canada: evidence from heterogeneous fabric development in the Onaping Formation and the Sudbury Igneous Complex. Journal of Structural Geology 29, 1744–1756.

Krogh, T.E., Davis, D.W., Corfu, F., 1984. Precise U-Pb zircon and Baddeleyite ages for the Sudbury area. In: Pye, E.G., Naldrett, A.J., Giblin, P.E. (Eds.), The Geology and Ore Deposits of the Sudbury Structure. Special Publication 1, Ontario Geological Survey, Toronto, pp. 431–446.

Kronenberg, A.K., Segall, P., Wolf, G.H., 1990. Hydrolytic weakening and penetrative deformation within a natural shear zone. Geophysical Monograph 56, 21–36.

Lightfoot, P.C., 2009. Mechanisms of Ni-Cu-PGE Sulphide Ore Formation in the Impact-Generated Sudbury Melt Sheet AGU Joint Assembly, abstract GA32B-04.

Means, W.D., 1989. Synkinematic microscopy of transparent polycrystals. Journal of Structural Geology 11, 163–174.

Milkereit, B., Green, A., Sudbury Working Group, 1992. Deep geometry of the Sudbury structure from seismic reflection profiling. Geology 20, 807–811.

Naldrett, A.J., Bray, J.G., Gasparrini, E.L., Podolsky, T., Rucklidge, J.C., 1970. Cryptic variation and the Petrology of the Sudbury Nickel Irruptive. Economic Geology and the Bulletin of the Society of Economic Geologists 65, 122–274.

Naldrett, A.J., Hewins, R.H., 1984. The Main Mass of the Sudbury Igneous Complex. In: Pye, E.G., Naldrett, A.J., Giblin, P.E. (Eds.), The Geology and Ore Deposits of the Sudbury Structure. Special Publication 1. Ontario Geological Survey, Toronto, pp. 235–252.

Pennacchioni, G., 2005. Control of the geometry of precursor brittle structures on the type of ductile shear zone in the Adamello tonalites, Southern Alps (Italy). Journal of Structural Geology 27, 627–644.

Peredery, W.V., Morrison, G.G., 1984. Discussion of the Origin of the Sudbury Structure. In: Pye, E.G., Naldrett, A.J., Giblin, P.E. (Eds.), The Geology and Ore Deposits of the Sudbury Structure. Special Publication 1, Ontario Geological Survey, Toronto, pp. 491–511.

Piercey, P., Schneider, D.A., Holm, D.K., 2007. Geochronology of Proterozoic metamorphism in the deformed Southern Province, northern Lake Huron region, Canada. Precambrian Research 157, 127–143.

Pye, E.G., Naldrett, A.J., Giblin, P.E. (Eds.), 1984. The Geology and Ore Deposits of the Sudbury Structure. Ontario Geological Survey, Special Volume 1, Toronto.

Riller, U., Schwerdtner, W., 1997. Mid-crustal deformation at the southern flank of the Sudbury Basin, central Ontario, Canada. Geological Society of America Bulletin 109, 841–854.

Riller, U., Schwerdtner, W.M., Robin, P.-Y.F., 1998. Low-temperature deformation mechanisms at a lithotectonic interface near the Sudbury Basin, Eastern Penokean Orogen, Canada. Tectonophysics 287, 59–75.

Riller, U., Schwerdtner, W., Halls, H., Card, K., 1999. Transpressive tectonism in the eastern Penokean orogen, Canada. Consequences for Proterozoic crustal kinematics and continental fragmentation. Precambrian Research 93, 51–70.

Riller, U., 2005. Structural characteristics of the Sudbury Impact Structure, Canada: impact-induced and orogenic deformation – a review. Meteoritics and Planetary Science 40, 1723–1740.

Riller, U., Boutelier, D., Schrank, C., Cruden, A.R., 2010. Role of kilometer-scale weak circular heterogeneities on upper crustal deformation patterns: evidence from scaled analogue modeling and the Sudbury Basin, Canada. Earth and Planetary Science Letters 297, 587–597.

Rousell, D.H., 1975. Origin of foliation and lineation in Onaping Formation and deformation of Sudbury Basin. Canadian Journal of Earth Sciences 12, 1379–1395.

Rousell, D.H., 1984. Structural Geology of the Sudbury Basin. In: Pye, E.G., Naldrett, A.J., Giblin, P.E. (Eds.), The Geology and Ore Deposits of the Sudbury Structure. Special Publication 1, Ontario Geological Survey, Toronto, pp. 83–95.

Segall, P., Simpson, C., 1986. Nucleation of ductile shear zones on dilatant fractures. Geology 14, 56–59. DOI: 10.1130/0091-7613(1986)14<56:NODSZO>2.0.CO;2.

Shanks, W.S., Schwerdtner, W.M., 1991. Structural analysis of the central and southwestern Sudbury Structure, Southern Province, Canadian Shield. Canadian Journal of Earth Sciences 28, 411–430.

Spray, J.G., Butler, H.R., Thompson, L.M., 2004. Tectonic influences on the morphometry of the Sudbury impact structure: implications for terrestrial cratering and modeling. Meteoritics and Planetary Science 39, 287–301.

Spang, J.H., 1972. Numerical method for dynamic analysis of calcite twin lamellae. Geological Society of America Bulletin 83, 467–471.

Thomson, M.L., Barnett, R.L., Fleet, M.E., Kerrich, R., 1985. Metamorphic assemblages in the South-Range Norite and the footwall mafic rocks near the Kirkwood mine, Sudbury, Ontario. The Canadian Mineralogist 23, 173–186.

Tourigny, G., Tremblay, A., 1997. Origin and incremental evolution of brittle/ductile shear zones in granitic rocks: natural examples from the southern Abitibi Belt, Canada. Journal of Structural Geology 19, 15–27.

Watts, M., Williams, G.D., 1979. Fault rocks as indicators of progressive shear deformation in Guingamp region, Brittany. Journal of Structural Geology 1, 323–332.

Wu, J.J., Milkereit, B., Boerner, D., 1994. Timing constraints on deformation history of the Sudbury Impact Structure. Canadian Journal of Earth Sciences 31, 1654–1660.